Article

INTERNATIONAL JOURNAL OF DAMAGE MECHANICS

International Journal of Damage Mechanics
0(0) 1–13

DOI: 10.1177/1056789518769343
journals.sagepub.com/home/ijd
SAGE

Strength nature of two-dimensional woven nanofabrics under biaxial tension

Yinfeng Li[1,2], Simanta Lahkar[1,3], Qingyuan Wei[1], Pizhong Qiao[1] and Han Ye[4]

Abstract

Woven nanostructures have been acknowledged as a platform for solar cells, supercapacitors, and sensors, making them especially of interest in the fields of materials sciences, nanotechnology, and renewable energy. By employing molecular dynamics simulations, the mechanical properties of two-dimensional woven nanofabrics under biaxial tension are evaluated. Two-dimensional woven nanostructures composed of graphene and graphyne nanoribbons are examined. Dynamic failure process of both graphene woven nanofabric and graphyne woven nanofabric with the same woven unit cell initiates at the edge of interlaced ribbons accompanied by the formation of cracks near the crossover location of yarns. Further stress analysis reveals that such failure mode is attributed to the compression between two overlaced ribbons and consequently their deformation under biaxial tension, which is sensitive to the lattice structure of nanoribbon as well as the density of yarns in fabric. Systemic comparisons between nanofabrics with different yarn width and interval show that the strength of nanofabric can be effectively controlled by tuning the space interval between nanoribbons. For nanofabrics with fixed large gap spacing, the strength of fabric does not change with the ribbon width, while the strength of nanofabric with small gap spacing decreases anomalously with the increase in yarn density. Such fabric strength dependency on gap spacing is the result of the stress concentration caused by the interlace compression. The outcomes of simulation suggest that the compacted arrangement of yarns in carbon woven nanofabric structures should be avoided to achieve high strength performance.

Keywords

Woven fabric, graphene, graphyne, biaxial tension, molecular dynamics simulation

[1]State Key Laboratory of Ocean Engineering, Department of Engineering Mechanics, School of Naval Architecture, Ocean and Civil Engineering, Shanghai Jiao Tong University, Shanghai, China
[2]Collaborative Innovation Center for Advanced Ship and Deep-Sea Exploration, Shanghai, China
[3]Department of Mechanical Engineering, Birla Institute of Technology & Science, Pilani Zuarinagar, Goa, India
[4]State Key Laboratory of Information Photonics and Optical Communications, Beijing University of Posts and Telecommunications, Beijing, China

Corresponding author:
Yinfeng Li, State Key Laboratory of Ocean Engineering, Department of Engineering Mechanics, School of Naval Architecture, Ocean and Civil Engineering, Shanghai Jiao Tong University, 800 Dongchuan Road, Shanghai, 200240 China.
Email: liyinfeng@sjtu.edu.cn

Introduction

Nanostructures, including graphene sheets, 3D network structures, nanoribbons, carbon nanotubes and woven fabrics, have been a field of extensive research with vast range of exciting applications in the field of electronics (Carretero–González et al., 2012; Gong et al., 2016; Liu et al., 2017; Pan et al., 2011; Weiss et al., 2012). As increasing research is being directed toward nanoelectronics, many new and promising 2D nanomaterials, other than graphene, have been proposed and developed, some of which include boron-nitride, graphyne and graphdiyne, transition metal dichalcogenides, and metal phosphorus trichalcogenides (Özçelik and Ciraci, 2013; Srinivasu and Ghosh, 2012; Tan et al., 2017; Yi et al., 2017). In particular, studies on graphyne sheets have shown that they are an excellent candidate in novel nanoelectronic and optoelectronic devices with highly tunable band gaps, large carrier mobility, and unique transport properties (Chen et al., 2013; Koo et al., 2013; Wu et al., 2013; Yue et al., 2013). These nanostructures have been explored for applications in flexible sensors due to their excellent electromechanical properties (Li et al., 2017; Liu et al., 2017; Weiss et al., 2012; Yang et al., 2014, 2015). Another popular area of their application has been developing efficient, light-weight, and flexible energy storage devices for effective use of renewable energy (He et al., 2013; Huang et al., 2012; Kim et al., 2015; Shi et al., 2013; Weiss et al., 2012; Wen et al., 2016; Xu et al., 2013; Zhang, Wang, et al., 2012; Zhu et al., 2012). Owing to their excellent photoelectric properties, extensive research has been done on application of these nanostructures in photodetectors and solar cells (Chen et al., 2016; Kouhnavard et al., 2015; Ma et al., 2018; Meng et al., 2015; Tian et al., 2017; Yang et al., 2013; Zhang, Wang, et al., 2012).

Of these, graphene woven fabric (GWF) has attracted a considerable amount of research interest in the recent years. GWF was shown to have excellent sensitivity over a wide strain range due to its incredible electromechanical features, highlighting the promising use of GWF-based sensor for various e-skin applications (Yang et al., 2015). GWF-based torsion sensor with high sensitivity has been prepared and demonstrated to have much higher torsion capacity than conventional optical fiber torsion sensor (Zhang, Pei, et al., 2012). GWF was incorporated into polydimethylsiloxane composite sensors to create skin mountable devices for wearable instrument (Liu et al., 2017). GWF composite films were prepared and found to possess high in-plane thermal conductivity, showing a promising use in cooling applications for modern electronics (Gong et al., 2016). These applications highlight the immensely beneficial properties of these nanostructures, primarily due to the interlaced ribbon configuration of the woven fabric.

With the growth in computational power over the last decade, it is now possible to use molecular dynamics (MD) method to gain a much deeper understanding of the properties and behavior of woven nanostructures. MD is a simulation technique that helps elucidate material characteristics at the nanoscale by modeling fundamental interactions between the atoms and molecules based on first principles, incorporating the nonlinearities with significant accuracy (Haile, 1992). It is a specially effective technique to study the mechanics of nanostructures and has been employed in previous studies to understand the unraveling mechanics in graphene (Zhang et al., 2017) and effect of vacancy defects in failure strength of graphene nanoribbons (GNRs) (Zhang et al., 2016a, 2016b). MD has also been used to study woven fabric-like nanostructures, made of interlaced nanoribbons of graphene, showing that these woven nanofabrics (WNFs) with sparsely packed ribbons have much superior flexibility, toughness, and stretch strength as compared to pristine graphene sheets (Zhang et al., 2015). These advantageous properties serve to buttress the application of WNF as a solid platform for electronic sensors, solar cells, and supercapacitors. However, in order to design practical applications of WNFs, there is a need to further understand the fracture mechanism of these fabrics, what are the characteristics of the fabric that affect its fracture and how does the ribbon width and interribbon spacing of the fabric specifically determine its strength. Our study

is aimed to answer these particular gaps in our understanding of the mechanical properties of WNF that has not yet been addressed till now in previous studies by carrying out MD simulations of WNF composed of 2D nanoribbons under biaxial tension. To find the relevance of simulations for different nanomaterials, WNF models made of both graphene and graphyne, which are carbon allotropes with different lattice structures, are developed. We have selected gamma graphyne for simulation because it has been fabricated successfully in experiments (Li et al., 2010; Qian et al., 2012) and also because of its higher fracture strength and density as compared to other allotropes of graphyne (Zhang, Pei, et al., 2012), and its promising thermo-electrical properties (Kang et al., 2011; Luo et al., 2011; Pan, Zhang, et al., 2011; Zhou et al., 2011) that have been reported in previous studies. It is found that both graphene and graphyne models undergo brittle fracture near the crossover of nanoribbons and share a similar trend in the properties; however, their exact magnitudes differ for the different lattice types and chemical bonding. In this study, we found an inverse relationship of the fabric strength with the density of woven structure. This agrees well with the results of Zhang et al. (2015) and helps to validate our simulation. Moreover, we calculated the stress field in the nanoribbons and used it to explain that the fracture occurs due to deformation of the nanoribbons. Additionally, we observe that the gap between the parallel nanoribbons is the critical factor in deciding the strength of WNF, while the width of the nanoribbons does not affect its strength. More specifically, there is a critical value of this gap interval, below which the tensile strength of the fabric falls drastically under biaxial loading.

Modeling and methodology

Graphene WNF (GWNF) is constructed with GNRs perpendicularly crossing each other. The GNR goes up and down between other GNRs and extends in the waving plane. The wave surface for the GNRs follows the sinusoidal function, and the carbon atoms are placed on the wave surface with lattice constant of 1.42 Å. Graphyne WNFs (GyWNFs) are constructed in the same way as GWNF. Unlike graphene, graphyne has three different carbon–carbon bond lengths (which are 1.19 Å, 1.48 Å, and 1.49 Å) that are specified to form the required lattice structure. The unit cell of WNF with periodic boundary along lateral directions is shown in Figure 1. The unit cell of WNF is composed of 2×2 GNRs arranged in two perpendicular (x and y) directions forming the warp and weft yarns, and it can be used to represent an infinite GWNF under periodic boundary conditions. The square holes are periodic and identical when the GNRs cross evenly, and the spacing interval between yarns of the GWNF can be tuned by changing the width of the GNRs as well as the size of the unit cell. WNFs with various yarn intervals are constructed in Ovito, an open-source

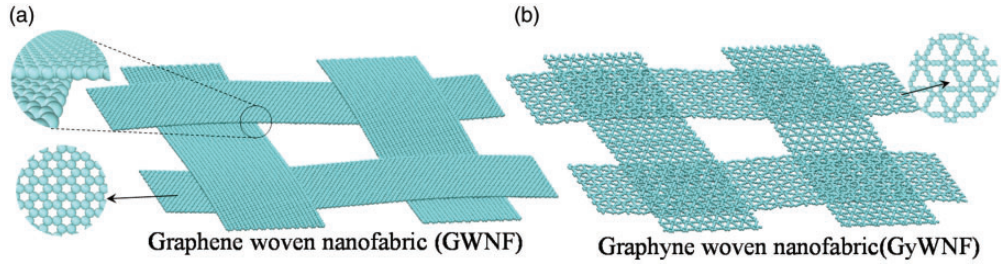

Figure 1. Atomistic structures of the unit cell of (a) graphene woven nanofabric (GWNF) and (b) graphyne woven nanofabric (GyWNF).

software (Alexander, 2010). Typically, square GWNF structures and GyWNF structures are built with same side length of 200 Å and varying ribbon widths of 50 Å, 60 Å, 70 Å, 80 Å, 90 Å, and 95 Å for the sake of comparison. After relaxation, models of GWNF with a side length about 201.11 Å and of GyWNF with a side length about 196.31 Å are obtained. Considering the crest will affect the stability of GWNF, the crest of GNRs in the model is 3.4 Å for stable fabric structure. For the height of the simulation box, any suitable value larger than 20 Å works fine to prevent the WNF interacting across the vertical periodic boundary.

In order to study the behavior of GWNF and GyWNF under biaxial tension, large-scale atomic/molecular massively parallel simulator (LAMMPS) (Plimpton, 1995) is used to conduct the molecular dynamics simulations. The adaptive intermolecular reactive empirical bond order (AIREBO) potential (Stuart et al., 2000) is adopted for the WNF models. The parameters of the potential are obtained from the CH.airebo file that comes with the LAMMPS installation folder. It should be noted that this potential is best suited for systems containing hydrogen and carbon atoms, which makes it accessible for all-carbon systems such as the ones being modeled in this study. The cutoff distance between carbons in CH.airebo is set as 1.92 Å as suggested in the literatures (Grantab et al., 2010; Li et al., 2015) to model bond formation and failure process properly, while the default cutoff distance of the airebo potential shows unreasonable interlayer bonding near the crossover location under biaxial tension as shown in Figure S1. The mass of carbon atoms is 12.0107 g/mol. The simulation box is set to have periodic boundaries in three dimensions. In the beginning, the total force and energy are minimized to get the optimum atomic coordinates. All the four edges with a width of 0.3 nm are fixed during relaxation where atoms in these edges are only allowed to move along z-direction. Then, the edges are unfixed, and the model moves freely for further equilibrium at 300 K before the tension is applied. Next, simulations are carried out under NVE (the number of particles, volume and total energy of the system is kept constant) ensemble based on Newtonian equations of motion using a standard velocity Verlet scheme of integration (Swope et al., 1982) with time step $\tau = 0.0001$ ps. The temperature is gradually increased from 1 K to room temperature at 0.01 K per time step using a Berendsen thermostat (Berendsen et al., 1984). Biaxial planar loading is applied to the sample by increasing the length and width of the simulation box and correspondingly remapping the x and y coordinates of the atoms. For the tensile test, a uniform strain is applied on the system at the rate of 0.02/ps. After 10 ps, the time step is changed to 0.001 ps and the strain rate is decreased to 0.01/ps until the ultimate failure of WNF.

Results and discussions

The specific woven structure of WNFs imbues certain special characteristics to it. The interlaced structure, obtained by the alternate crossing over of the warp and weft ribbons, provides resistance to displacement of the nanoribbons, enforcing the strength of the fabric. The overlapping of the warp and weft yarns near the crossing over point creates friction between them and thus restricts free motion of the ribbons. However, since the atoms in one ribbon at the interface between the overlapped yarns are not covalently bonded to the ones in the other ribbon, and they interact only through van der Waals interaction, it allows relative shifting of the ribbons during biaxial tension. As a result, the WNFs can undergo significant deformation before complete fracture. Thus, the special structure of woven materials, along with the properties of graphene, makes GWNFs a potential platform with high thermal conductivity and high sensitivity to strain for multitude of promising applications like in flexible electronics, strain sensors, supercapacitors, and solar cells (Gong et al., 2016; Liu et al., 2017; Yang et al., 2014, 2015). The weaving nature of WNFs is also responsible for interesting critical strength behavior of these structures under tensile loading.

The strength of WNFs is of particular relevance for their different applications. Here, the dynamic failure process of the WNF structures under biaxial tensile test is investigated until the point where the woven fabric undergoes complete fracture (Video S1). The snapshots taken from the failure process of GWNF composed of four unit cells is shown in Figure 2. The fracture of GWNF initiates near the points of crossover between warp and weft ribbons, showing that the crossover regions of the ribbons are the most vulnerable location for initiation of fracture under biaxial tension. There is no necking in the ribbons before fracture, which indicates that the ribbons undergo brittle fracture under the applied biaxial tension. GyWNF composed of graphyne nanoribbons fracture in a similar brittle manner which is a characteristic feature of the fracture mechanism in WNFs. These results agree with a previous study that reported similar failure modes in GWNFs (Zhang et al., 2015). Understanding the failure mechanism in woven structures would better assist in designing and controlling the failure process in WNF-based devices, as attempted later in this paper.

The strength manipulation of these WNFs based on the described failure mode is conducted. The effect of yarn density on the extent to which they can withstand stress before fracture occurs is first investigated. The density of yarns in WNF models is characterized by two parameters: the ribbon width w and gap spacing between nanoribbons w' as illustrated in Figure 3. The WNF models with same size but varying nanoribbon width and gap spacing are constructed for comparison. The models with larger w and smaller w' have higher yarn density, while the ones with smaller w and larger w' have lower densities. The calculated stress–strain curves of these GWNFs under biaxial tension are plotted in Figure 4(a). Besides the irregular fluctuations in measured stress response of the models at low strain, which may arise from the pressure uncertainties in the initial state of the

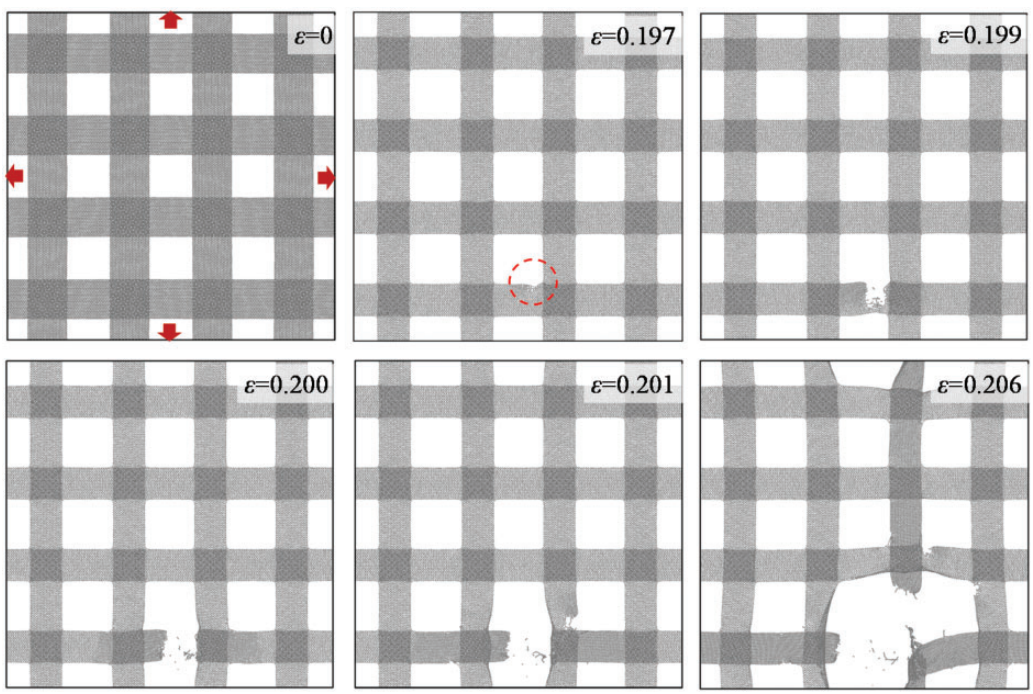

Figure 2. Snapshots take from the dynamics failure process of graphene woven fabric with four unit cells (a size of 40×40 nm) under biaxial loading.

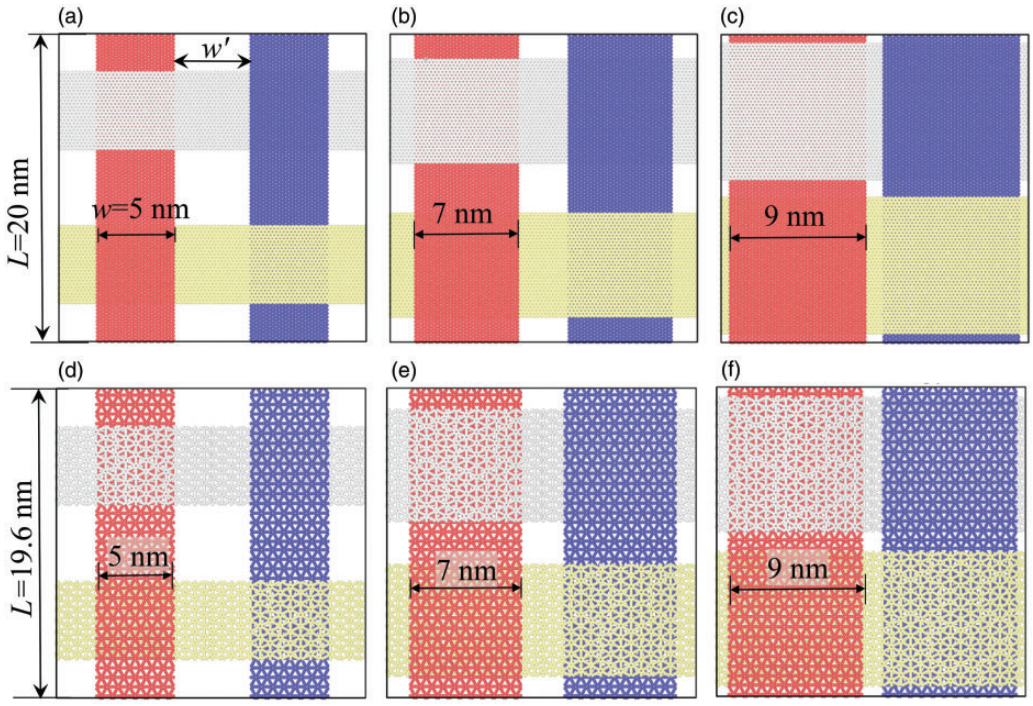

Figure 3. Atomistic structures of graphene woven fabrics (a–c) and graphyne woven fabrics (d–f) with varying ribbon width w and gap spacing $w' = L/2 - w$.

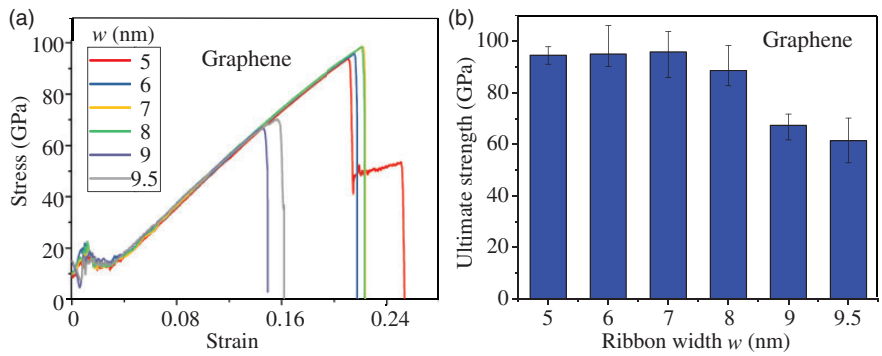

Figure 4. (a) The stress strain curves of graphene woven fabrics with varying ribbon width w and gap width $w' = L/2 - w$. (b) The ultimate strengths obtained from the peak value of stress strain curves.

system, the GWNFs show a linear variation of stress with strain over a significant region before failure. The average stiffness, as the slope of this linear elastic region, is similar for all the WNFs of a particular material irrespective of the yarn density of the woven structures. There is, however, an interesting correlation between the yarn density and the strength of WNF, which is estimated as the peak value of stress–strain curve.

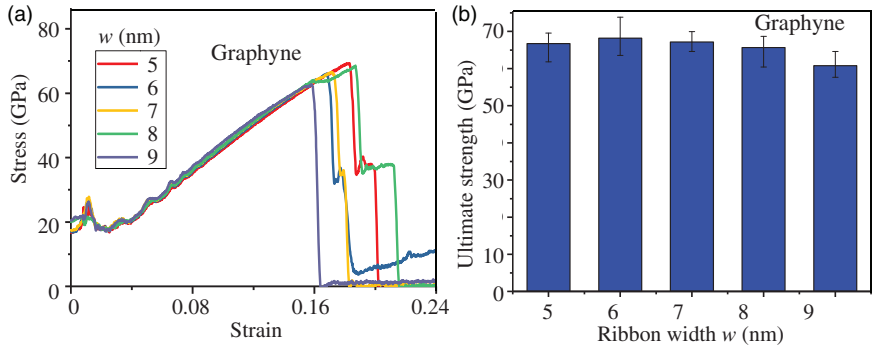

Figure 5. (a) The stress strain curves of graphyne woven fabrics with varying ribbon width w and gap spacing $w' = L/2 - w$. (b) The ultimate strengths obtained from the peak value of stress strain curves.

To measure the strength variation of the WNFs reliably, multiple replicas of each model with different durations of relaxation before the tensile test are performed. Thus, the replicas have slightly different initial states before loading, and the average of all the results for each WNF model is taken. The average strength of GWNFs from six independent simulations is plotted in Figure 4(b), and the error bars in the figure shows the deviations of measurements in the ensemble of results. Interestingly, for models with higher yarn densities, the strength of GWNF decreases drastically with the increase in density, while the strength of models with lower yarn densities is insensitive to the change. This shows that the yarn density is crucial in determining the WNF strength and a negative correlation between the strength and yarn density is demonstrated. In Figure 4(b), there exists a critical limit for WNF density beyond which the strength of GWNF can be controlled by varying its density. Hence, to secure better strength output, much high densities of the graphene fabric would in fact be less desirable.

The same fracture tests under biaxial tension are repeated to similar GyWNF models with varying densities, and the calculated stress–strain response is plotted in Figure 5(a). Similar to the case of graphene, the measured stiffness for GyWNF is also independent of the fabric density, while the strength decreases with the increase in density for GyWNFs with high density. However, the decrease in strength with density is much less prominent. The critical density of GyWNF, which can enable density-tuned strength of the fabric, seems to be higher than that of GWNF. Such mechanical difference between the WNF models of graphene and graphyne shows that the critical values for density to allow tuning of strength are sensitive to the lattice structure of nanoribbons. Thus, the density of yarns is crucial to the mechanical strength response of the WNFs, especially for GWNF.

By considering the peculiar variation of fracture strength with the yarn density of woven structures, the stress distribution in the unit cells during the biaxial tension is analyzed to better understand the fracture mechanism in WNFs. In the MD simulation, the virial stress (Pei et al., 2010) is calculated for every atom in the fabric model at different strain values. Because the models are symmetrical in the x (horizontal) and y (vertical) directions, the stress only in x-direction is measured. The stress contours of components σ_x in both graphene and graphyne models at particular strain values are shown in Figure 6 for illustration. Under biaxial tensile loading, almost all the atoms close to the region where two ribbons in warp and weft directions cross each other have a relatively higher stress value. Such a high stress concentration at the points near the crossover explains the observation that failure in the ribbons always initiates from that region during the

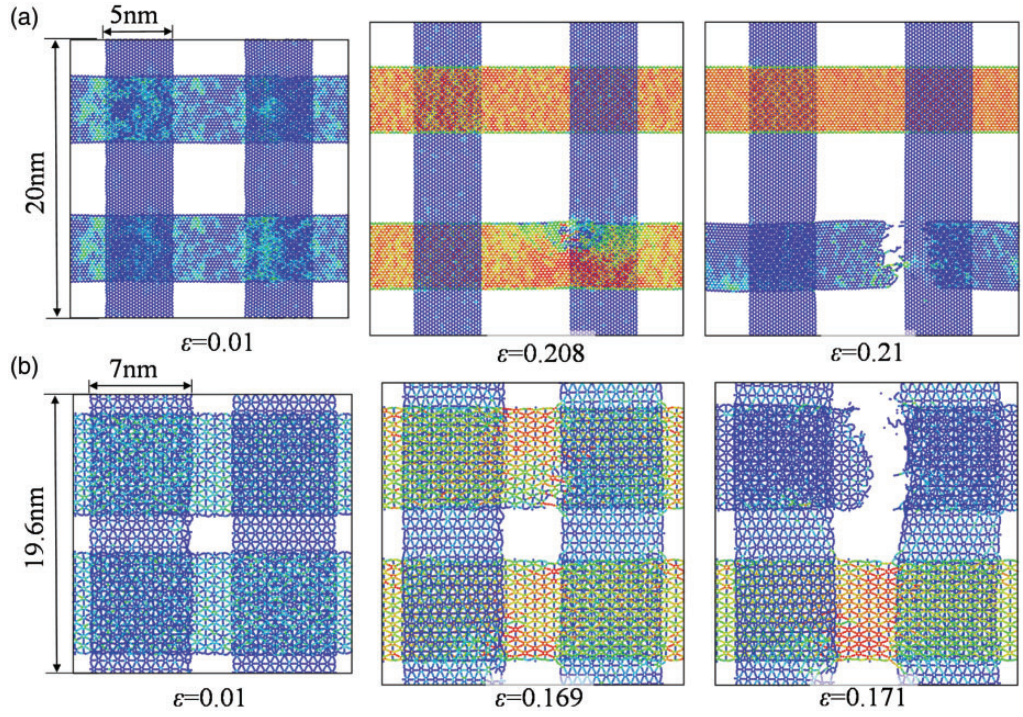

Figure 6. The evolution of stress distribution of σ_x with the strain for (a) graphene woven fabrics with $w = 5$ nm and (*b*) graphyne woven fabrics with $w = 7$ nm under biaxial loading.

biaxial tensile tests. Due to the interlaced arrangement, the weft and warp ribbons exert a pressing force on each other, which is orthogonal to the fabric plane and in opposite directions for adjacent crossover regions. This creates a shear effect in a ribbon in the gap between the crossovers. With increase in tension in the ribbons, the curvature close to the crossover region increases, while the ribbons pressed against each other come closer and repel each other more strongly. Hence, with the increased bending and shear deformation, the shear stress at the edge of the crossover also increases leading to the stress concentration. This residual stress effect in the ribbons finally leads to failure near crossover. With increasing yarn density, the decrease of gap distance between adjacent ribbons results in a higher shear affect over shorter distance due to increased bending and deformation, making the ribbons more susceptible to failure. Thus, failure caused by the shear deformation near the cross over edge helps explain why the fracture strength of the GWNFs decreases with the increase in yarn density. The clear knowledge of this fracture mechanism in WNFs is useful in designing graphene woven structures with optimal overall stress-bearing capacity.

To design optimum graphene woven structures, it is important to understand which of the two parameters that determined the density is more influential in affecting the strength of the fabric. Thus, more simulations are conducted to reevaluate the effect of the gap distance between adjacent ribbons. By fixing the overall size of the unit cell and decreasing the gap between the adjacent ribbons progressively by moving the ribbons closer, there is high stress concentration near the crossover region beside the gap. The maximum average stresses at the onset before the initiation of failure are shown in Figure 7 for illustration. The fracture strength of the woven structures significantly falls, as the size of the gap between the adjacent ribbons decreases. As the gap spacing

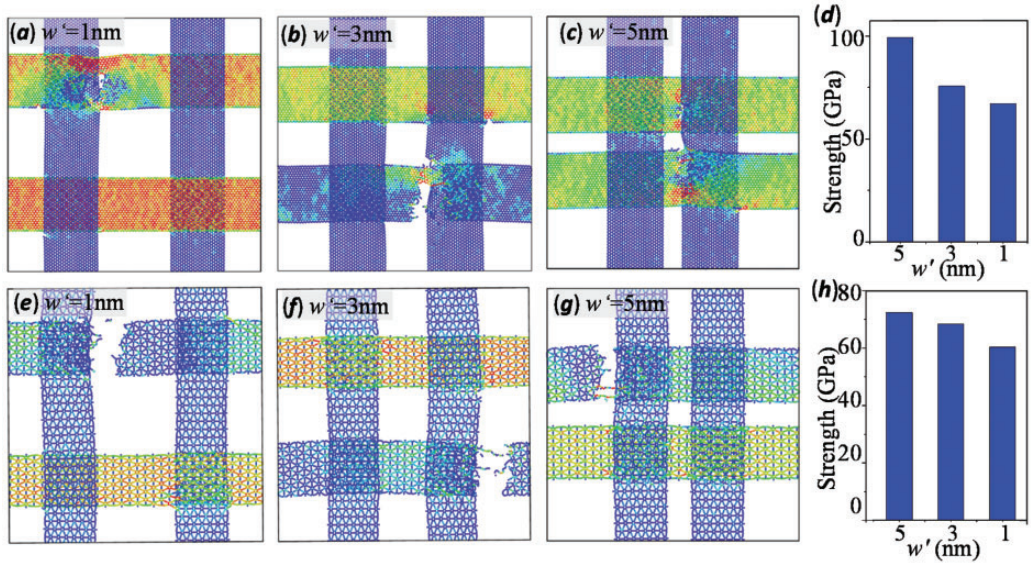

Figure 7. Influence of gap spacing on the stress distributions of σ_x in graphene woven fabrics (a–c) and graphyne woven fabrics (e–g) with fixed overall size *L*. (d) and (h) Changes of ultimate strength with the decrease of gap spacing for GWNF and GyWNF, respectively.

decreases from 5 nm to 1 nm, the deterioration of fracture strength is up to almost 40%. Similarly, there is also a significant strength decrease for the case of graphyne models though the change magnitude is not as high as the case of graphene. This implies that a densely woven fabric will have lower capacity to bear loads under biaxial tension than a WNF with lower packing density. Hence, the spacing between nanoribbons, or the packing density of nanoribbons, of WNFs plays a crucial role in determining the strength, and relatively loosely woven fabrics seem to fair better in tension. This agrees well with our preceding explanation of fracture occurring as a result of bending and increased shear deformation near crossover. Hence, the gap spacing of nanoribbons is a crucial control parameter that can be used to tune the mechanical properties of WNFs for various applications.

Next, the effect of width of nanoribbons on the tensile strength of WNFs is evaluated. To do that, WNF models with homogeneous ribbons of different widths are constructed, while keeping the gap spacing between adjacent ribbons the same for all the models, as illustrated in Figure 8(a) to (f). The comparison between the calculated strengths of these WNFs under biaxial tensile tests is shown in Figure 8(g). It is observed that there is no monotonic change in the fracture strength of both the GWNFs and GyWNFs with increasing ribbon width. The variation in strength of the fabric model is less than 5% as the width of nanoribbons increases from 5 nm to 7 nm for graphene models and 5 nm to 9 nm for graphyne models. This indicates that the change of the yarn width does not affect the mechanical strength of the WNFs when the gap distance is larger than a critical value as discussed in Figure 4. Hence, the nanoribbon density in WNF structures is in fact the critical factor that plays a key role in determining the load-bearing capacity of the fabric, and the strength of these woven fabrics can be adjusted based on the needs by changing the packing density of the WNF. Moreover, the WNFs with lower yarn densities have much higher strength owing to interlace interaction of the graphene fabric, which can be viewed as an important characteristic for various modern electronic devices.

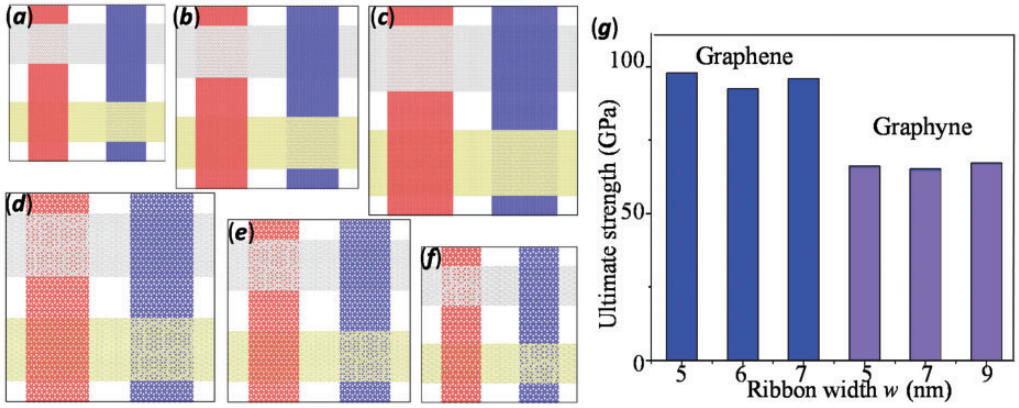

Figure 8. Comparisons between strength of woven fabrics under biaxial tension with fixed gap spacing w' but different ribbon width w. (a–c) Atomistic structures of graphene woven fabrics with $w' = 5$ nm and $w = 5, 7, 9$ nm, respectively. (d–f) Atomistic structures of graphyne woven fabrics with $w' = 5$ nm and $w = 9, 7, 5$ nm, respectively. (g) Dependency of strength on the increase in ribbon width.

Conclusions

In this study, the critical failure properties of the WNF structures using MD simulations are evaluated. The failure characteristics of the WNF under biaxial tension are studied to better understand the influence of various features on its failure response and to tune the mechanical properties of the woven fabric. This study shows that the yarn density of the GWNF has an interesting inverse effect on the strength of the fabric, i.e. the strength of the WNF falls with increase in density. It is further noted that the nanoribbon packing density of the woven fabric is crucial to determine its strength, and beyond a certain critical density, the strength of the fabric begins to falls significantly. We have explained the typical fracture behavior of the woven fabric as owing to the shear deformation near the overlap of the ribbons. In addition to these, the width of the nanoribbons has been shown to not affect the failure strength of the WNFs effectively. These properties thus show great significance to tune and adjust the mechanical properties of WNFs. Extended simulations can be conducted for WNF models of greater size range to verify the trends as observed in this study.

Acknowledgments

The computational support for this work was provided by Center for High Performance Computing, Shanghai Jiao Tong University.

Declaration of Conflicting Interests

The author(s) declared no potential conflicts of interest with respect to the research, authorship, and/or publication of this article.

Funding

The authors gratefully acknowledge the support of the National Natural Science Foundation of China (No. 11402145), the Open Fund of State Key Laboratory of Information Photonics and Optical Communications (Beijing University of Posts and Telecommunications) (IPOC2017B009), and the Medical-Engineering Cross Fund of Shanghai Jiao Tong University (YG2015MS13, YG2017QN64).

Supplementary Material

Supplementary material for this article is available online.

References

Alexander S (2010) Visualization and analysis of atomistic simulation data with OVITO—The open visualization tool. *Modelling and Simulation in Materials Science and Engineering* 18: 015012.

Berendsen HJC, Postma JPM, van Gunsteren WF, et al. (1984) Molecular dynamics with coupling to an external bath. *The Journal of Chemical Physics* 81: 3684–3690.

Carretero–González J, Castillo–Martínez E, Dias–Lima M, et al. (2012) Oriented graphene nanoribbon yarn and sheet from aligned multi-walled carbon nanotube sheets. *Advanced Materials* 24: 5695–5701.

Chen H, Liu H, Zhang Z, et al. (2016) Nanostructured photodetectors: From ultraviolet to terahertz. *Advanced Materials* 28: 403–433.

Chen J, Xi J, Wang D, et al. (2013) Carrier mobility in graphyne should be even larger than that in graphene: A theoretical prediction. *The Journal of Physical Chemistry Letters* 4: 1443–1448.

Gong J, Liu Z, Yu J, et al. (2016) Graphene woven fabric-reinforced polyimide films with enhanced and anisotropic thermal conductivity. *Composites Part A: Applied Science and Manufacturing* 87: 290–296.

Grantab R, Shenoy VB and Ruoff RS (2010) Anomalous strength characteristics of tilt grain boundaries in graphene. *Science* 330: 946–948.

Haile JM (1992). *Molecular Dynamics Simulation: Elementary Methods*. New York: John Wiley & Sons.

He Y, Chen W, Li X, et al. (2013) Freestanding three-dimensional graphene/MnO_2 composite networks as ultralight and flexible supercapacitor electrodes. *ACS Nano* 7: 174–182.

Huang Y, Liang J and Chen Y (2012) An overview of the applications of graphene-based materials in supercapacitors. *Small* 8: 1805–1834.

Kang J, Li J, Wu F, et al. (2011) Elastic, electronic, and optical properties of two-dimensional graphyne sheet. *The Journal of Physical Chemistry C* 115: 20466–20470.

Kim BC, Hong J-Y, Wallace GG, et al. (2015) Recent progress in flexible electrochemical capacitors: Electrode materials, device configuration, and functions. *Advanced Energy Materials* 5: 1500959.

Koo J, Hwang HJ, Huang B, et al. (2013) Exotic geometrical and electronic properties in hydrogenated graphyne. *The Journal of Physical Chemistry C* 117: 11960–11967.

Kouhnavard M, Ludin NA, Ghaffari BV, et al. (2015) Carbonaceous materials and their advances as a counter electrode in dye-sensitized solar cells: Challenges and prospects. *ChemSusChem* 8: 1510–1533.

Li G, Li Y, Liu H, et al. (2010) Architecture of graphdiyne nanoscale films. *Chemical Communications* 46: 3256–3258.

Li R, Si Y, Zhu Z, et al. (2017) Supercapacitive iontronic nanofabric sensing. *Advanced Materials* 29: 1700253.

Li Y, Datta D and Li Z (2015) Anomalous mechanical characteristics of graphene with tilt grain boundaries tuned by hydrogenation. *Carbon* 90: 234–241.

Liu X, Tang C, Du X, et al. (2017) A highly sensitive graphene woven fabric strain sensor for wearable wireless musical instruments. *Materials Horizons* 4: 477–486.

Luo G, Qian X, Liu H, et al. (2011) Quasiparticle energies and excitonic effects of the two-dimensional carbon allotrope graphdiyne: Theory and experiment. *Physical Review B* 84: 075439.

Ma D, Li T, Xu Z, et al. (2018) Electrochromic devices based on tungsten oxide films with honeycomb-like nanostructures and nanoribbons array. *Solar Energy Materials and Solar Cells* 177: 51–56.

Meng X, Yu C, Song X, et al. (2015) Nitrogen-doped graphene nanoribbons with surface enriched active sites and enhanced performance for dye-sensitized solar cells. *Advanced Energy Materials* 5: 1500180.

Özçelik VO and Ciraci S (2013) Size dependence in the stabilities and electronic properties of α-graphyne and its boron nitride analogue. *The Journal of Physical Chemistry C* 117: 2175–2182.

Pan LD, Zhang LZ, Song BQ, et al. (2011) Graphyne- and graphdiyne-based nanoribbons: Density functional theory calculations of electronic structures. *Applied Physics Letters* 98: 173102.

Pan Z, Liu N, Fu L, et al. (2011) Wrinkle engineering: A new approach to massive graphene nanoribbon arrays. *Journal of the American Chemical Society* 133: 17578–17581.

Pei Q, Zhang Y and Shenoy V (2010) A molecular dynamics study of the mechanical properties of hydrogen functionalized graphene. *Carbon* 48: 898–904.

Plimpton S (1995) Fast parallel algorithms for short-range molecular dynamics. *Journal of Computational Physics* 117: 1–19.

Qian X, Ning Z, Li Y, et al. (2012) Construction of graphdiyne nanowires with high-conductivity and mobility. *Dalton Transactions* 41: 730–733.

Shi Y, Chou S-L, Wang J-Z, et al. (2013) In-situ hydrothermal synthesis of graphene woven VO_2 nanoribbons with improved cycling performance. *Journal of Power Sources* 244: 684–689.

Srinivasu K and Ghosh SK (2012) Graphyne and graphdiyne: Promising materials for nanoelectronics and energy storage applications. *The Journal of Physical Chemistry C* 116: 5951–5956.

Stuart SJ, Tutein AB and Harrison JA (2000) A reactive potential for hydrocarbons with intermolecular interactions. *The Journal of Chemical Physics* 112: 6472–6486.

Swope WC, Andersen HC, Berens PH, et al. (1982) A computer simulation method for the calculation of equilibrium constants for the formation of physical clusters of molecules: Application to small water clusters. *The Journal of Chemical Physics* 76: 637–649.

Tan C, Cao X, Wu X-J, et al. (2017) Recent advances in ultrathin two-dimensional nanomaterials. *Chemical Reviews* 117: 6225–6331.

Tian W, Liu D, Cao F, et al. (2017) Hybrid nanostructures for photodetectors. *Advanced Optical Materials* 5: 1600468.

Weiss NO, Zhou H, Liao L, et al. (2012) Graphene: An emerging electronic material. *Advanced Materials* 24: 5782–5825.

Wen L, Li F and Cheng H-M (2016) Carbon nanotubes and graphene for flexible electrochemical energy storage: From materials to devices. *Advanced Materials* 28: 4306–4337.

Wu W, Guo W and Zeng XC (2013) Intrinsic electronic and transport properties of graphyne sheets and nanoribbons. *Nanoscale* 5: 9264–9276.

Xu J, Wang Q, Wang X, et al. (2013) Flexible asymmetric supercapacitors based upon Co_9S_8 nanorod// $Co_3O_4@RuO_2$ nanosheet Arrays on carbon cloth. *ACS Nano* 7: 5453–5462.

Yang T, Wang W, Zhang H, et al. (2015) Tactile sensing system based on arrays of graphene woven microfabrics: Electromechanical behavior and electronic skin application. *ACS Nano* 9: 10867–10875.

Yang T, Wang Y, Li X, et al. (2014) Torsion sensors of high sensitivity and wide dynamic range based on a graphene woven structure. *Nanoscale* 6: 13053–13059.

Yang Z, Liu M, Zhang C, et al. (2013) Carbon nanotubes bridged with graphene nanoribbons and their use in high-efficiency dye-sensitized solar cells. *Angewandte Chemie International Edition* 52: 3996–3999.

Yi W-c, Liu W, Botana J, et al. (2017) Honeycomb boron allotropes with dirac cones: A true analogue to graphene. *The Journal of Physical Chemistry Letters* 8: 2647–2653.

Yue Q, Chang S, Kang J, et al. (2013) Mechanical and electronic properties of graphyne and its family under elastic strain: Theoretical predictions. *The Journal of Physical Chemistry C* 117: 14804–14811.

Zhang J, Tarek R and Cemal B (2016a) Influence of vacancy defects on the damage mechanics of graphene nanoribbons. *International Journal of Damage Mechanics* 26: 29–49.

Zhang J, Tarek R and Cemal B (2016b) The effects of vacancy defect on the fracture behaviors of zigzag graphene nanoribbons. *International Journal of Damage Mechanics* 26: 608–630.

Zhang L, Becton M and Wang X (2015) Mechanical analysis of graphene-based woven nano-fabric. *Materials Science and Engineering: A* 620: 367–374.

Zhang W, Ragab T and Basaran C (2017) Unraveling mechanics of armchair and zigzag graphene nanoribbons. *International Journal of Damage Mechanics* 26: 447–462.

Zhang X, Wang B, Sunarso J, et al. (2012) Graphene nanostructures toward clean energy technology applications. *Wiley Interdisciplinary Reviews: Energy and Environment* 1: 317–336.

Zhang YY, Pei QX and Wang CM (2012) Mechanical properties of graphynes under tension: A molecular dynamics study. *Applied Physics Letters* 101: 081909.

Zhou J, Lv K, Wang Q, et al. (2011) Electronic structures and bonding of graphyne sheet and its BN analog. *The Journal of Chemical Physics* 134: 174701.

Zhu Y, James DK and Tour JM (2012) New routes to graphene, graphene oxide and their related applications. *Advanced Materials* 24: 4924–4955.